

Cavity quantum electrodynamics for superconducting electrical circuits: An architecture for quantum computation

Alexandre Blais,¹ Ren-Shou Huang,^{1,2} Andreas Wallraff,¹ S. M. Girvin,¹ and R. J. Schoelkopf¹

¹*Departments of Physics and Applied Physics, Yale University, New Haven, Connecticut 06520, USA*

²*Department of Physics, Indiana University, Bloomington, Indiana 47405, USA*

(Received 7 February 2004; published 29 June 2004; corrected 23 July 2004)

We propose a realizable architecture using one-dimensional transmission line resonators to reach the strong-coupling limit of cavity quantum electrodynamics in superconducting electrical circuits. The vacuum Rabi frequency for the coupling of cavity photons to quantized excitations of an adjacent electrical circuit (qubit) can easily exceed the damping rates of both the cavity and qubit. This architecture is attractive both as a macroscopic analog of atomic physics experiments and for quantum computing and control, since it provides strong inhibition of spontaneous emission, potentially leading to greatly enhanced qubit lifetimes, allows high-fidelity quantum nondemolition measurements of the state of multiple qubits, and has a natural mechanism for entanglement of qubits separated by centimeter distances. In addition it would allow production of microwave photon states of fundamental importance for quantum communication.

DOI: 10.1103/PhysRevA.69.062320

PACS number(s): 03.67.Lx, 73.23.Hk, 74.50.+r, 32.80.-t

I. INTRODUCTION

Cavity quantum electrodynamics (CQED) studies the properties of atoms coupled to discrete photon modes in high Q cavities. Such systems are of great interest in the study of the fundamental quantum mechanics of open systems, the engineering of quantum states, and measurement-induced decoherence [1–3] and have also been proposed as possible candidates for use in quantum information processing and transmission [1–3]. Ideas for novel CQED analogs using nanomechanical resonators have recently been suggested by Schwab and collaborators [4,5]. We present here a realistic proposal for CQED via Cooper pair boxes coupled to a one-dimensional (1D) transmission line resonator, within a simple circuit that can be fabricated on a single microelectronic chip. As we discuss, 1D cavities offer a number of practical advantages in reaching the strong-coupling limit of CQED over previous proposals using discrete LC circuits [6,7], large Josephson junctions [8–10], or 3D cavities [11–13]. Besides the potential for entangling qubits to realize two-qubit gates addressed in those works, in the present work we show that the CQED approach also gives strong and controllable isolation of the qubits from the electromagnetic environment, permits high-fidelity quantum nondemolition (QND) readout of multiple qubits, and can produce states of microwave photon fields suitable for quantum communication. The proposed circuits therefore provide a simple and efficient architecture for solid-state quantum computation, in addition to opening up a new avenue for the study of entanglement and quantum measurement physics with macroscopic objects. We will frame our discussion in a way that makes contact between the language of atomic physics and that of electrical engineering.

We begin in Sec. II with a brief general overview of CQED before turning to a discussion of our proposed solid-state realization of cavity QED in Sec. III. We then discuss in Sec. IV the case where the cavity and qubit are tuned in resonance and in Sec. V the case of large detuning which

leads to lifetime enhancement of the qubit. In Sec. VI, a quantum nondemolition readout protocol is presented. Realization of one-qubit logical operations is discussed in Sec. VII and two-qubit entanglement in Sec. VIII. We show in Sec. IX how to take advantage of encoded universality and decoherence-free subspace in this system.

II. BRIEF REVIEW OF CAVITY QED

Cavity QED studies the interaction between atoms and the quantized electromagnetic modes inside a cavity. In the optical version of CQED [2], schematically shown in Fig. 1(a), one drives the cavity with a laser and monitors changes in the cavity transmission resulting from coupling to atoms falling through the cavity. One can also monitor the spontaneous emission of the atoms into transverse modes not confined by the cavity. It is not generally possible to directly determine the state of the atoms after they have passed through the cavity because the spontaneous emission lifetime is on the scale of nanoseconds. One can, however, infer information about the state of the atoms inside the cavity from real-time monitoring of the cavity optical transmission.

In the microwave version of CQED [3], one uses a very-high- Q superconducting 3D resonator to couple photons to transitions in Rydberg atoms. Here one does not directly monitor the state of the photons, but is able to determine with high efficiency the state of the atoms after they have passed through the cavity (since the excited state lifetime is of the order of 30 ms). From this state-selective detection one can infer information about the state of the photons in the cavity.

The key parameters describing a CQED system (see Table I) are the cavity resonance frequency ω_c , the atomic transition frequency Ω , and the strength of the atom-photon coupling g appearing in the Jaynes-Cummings Hamiltonian [14]

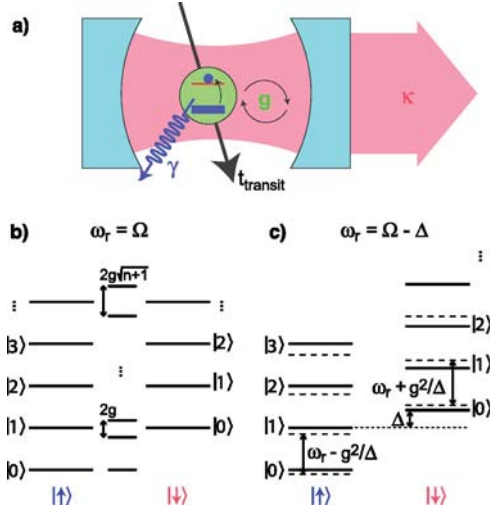


FIG. 1. (Color online) (a) Standard representation of a cavity quantum electrodynamics system, comprising a single mode of the electromagnetic field in a cavity with decay rate κ coupled with a coupling strength $g = \mathcal{E}_{\text{rms}} d / \hbar$ to a two-level system with spontaneous decay rate γ and cavity transit time t_{transit} . (b) Energy spectrum of the uncoupled (left and right) and dressed (center) atom-photon states in the case of zero detuning. The degeneracy of the two-dimensional manifolds of states with $n-1$ quanta is lifted by $2g\sqrt{n+1}$. (c) Energy spectrum in the dispersive regime (long-dashed lines). To second order in g , the level separation is independent of n , but depends on the state of the atom.

$$H = \hbar\omega_r \left(a^\dagger a + \frac{1}{2} \right) + \frac{\hbar\Omega}{2} \sigma^z + \hbar g (a^\dagger \sigma^- + \sigma^+ a) + H_\kappa + H_\gamma. \quad (1)$$

Here H_κ describes the coupling of the cavity to the continuum which produces the cavity decay rate $\kappa = \omega_r / Q$, while H_γ describes the coupling of the atom to modes other than the cavity mode which cause the excited state to decay at rate γ (and possibly also produce additional dephasing effects). An additional important parameter in the atomic case is the

transit time t_{transit} of the atom through the cavity.

In the absence of damping, exact diagonalization of the Jaynes-Cummings Hamiltonian yields the excited eigenstates (dressed states) [15]

$$|+\rangle, n\rangle = \cos \theta_n |\downarrow, n\rangle + \sin \theta_n |\uparrow, n+1\rangle, \quad (2)$$

$$|-\rangle, n\rangle = -\sin \theta_n |\downarrow, n\rangle + \cos \theta_n |\uparrow, n+1\rangle, \quad (3)$$

and ground state $|\uparrow, 0\rangle$ with corresponding eigenenergies

$$E_{\pm, n} = (n+1)\hbar\omega_r \pm \frac{\hbar}{2} \sqrt{4g^2(n+1) + \Delta^2}, \quad (4)$$

$$E_{\uparrow, 0} = -\frac{\hbar\Delta}{2}. \quad (5)$$

In these expressions,

$$\theta_n = \frac{1}{2} \tan^{-1} \left(\frac{2g\sqrt{n+1}}{\Delta} \right), \quad (6)$$

and $\Delta \equiv \Omega - \omega_r$ the atom-cavity detuning.

Figure 1(b) shows the spectrum of these dressed states for the case of zero detuning, $\Delta = 0$, between the atom and cavity. In this situation, degeneracy of the pair of states with $n+1$ quanta is lifted by $2g\sqrt{n+1}$ due to the atom-photon interaction. In the manifold with a single excitation, Eqs. (2) and (3) reduce to the maximally entangled atom-field states $|\pm, 0\rangle = (|\uparrow, 1\rangle \pm |\downarrow, 0\rangle) / \sqrt{2}$. An initial state with an excited atom and zero photons $|\uparrow, 0\rangle$ will therefore flop into a photon $|\downarrow, 1\rangle$ and back again at the vacuum Rabi frequency g/π . Since the excitation is half atom and half photon, the decay rate of $|\pm, 0\rangle$ is $(\kappa + \gamma)/2$. The pair of states $|\pm, 0\rangle$ will be resolved in a transmission experiment if the splitting $2g$ is larger than this linewidth. The value of $g = \mathcal{E}_{\text{rms}} d / \hbar$ is determined by the transition dipole moment d and the rms zero-point electric field of the cavity mode. Strong coupling is achieved when $g \gg \kappa, \gamma$ [15].

TABLE I. Key rates and CQED parameters for optical [2] and microwave [3] atomic systems using 3D cavities, compared against the proposed approach using superconducting circuits, showing the possibility for attaining the strong cavity QED limit ($n_{\text{Rabi}} \gg 1$). For the 1D superconducting system, a full-wave ($L = \lambda$) resonator, $\omega_r / 2\pi = 10$ GHz, a relatively low Q of 10^4 , and coupling $\beta = C_g / C_\Sigma = 0.1$ are assumed. For the 3D microwave case, the number of Rabi flops is limited by the transit time. For the 1D circuit case, the intrinsic Cooper-pair box decay rate is unknown; a conservative value equal to the current experimental upper bound $\gamma \leq 1/(2 \mu\text{s})$ is assumed.

Parameter	Symbol	3D optical	3D microwave	1D circuit
Resonance or transition frequency	$\omega_r / 2\pi, \Omega / 2\pi$	350 THz	51 GHz	10 GHz
Vacuum Rabi frequency	$g / \pi, g / \omega_r$	220 MHz, 3×10^{-7}	47 kHz, 1×10^{-7}	100 MHz, 5×10^{-3}
Transition dipole	d / ea_0	~ 1	1×10^3	2×10^4
Cavity lifetime	$1 / \kappa, Q$	10 ns, 3×10^7	1 ms, 3×10^8	160 ns, 10^4
Atom lifetime	$1 / \gamma$	61 ns	30 ms	$2 \mu\text{s}$
Atom transit time	t_{transit}	$\geq 50 \mu\text{s}$	100 μs	∞
Critical atom number	$N_0 = 2\gamma\kappa / g^2$	6×10^{-3}	3×10^{-6}	$\leq 6 \times 10^{-5}$
Critical photon number	$m_0 = \gamma^2 / 2g^2$	3×10^{-4}	3×10^{-8}	$\leq 1 \times 10^{-6}$
Number of vacuum Rabi flops	$n_{\text{Rabi}} = 2g / (\kappa + \gamma)$	~ 10	~ 5	$\sim 10^2$

For large detuning, $g/\Delta \ll 1$, expansion of Eq. (4) yields the dispersive spectrum shown in Fig. 1(c). In this situation, the eigenstates of the one excitation manifold take the form [15]

$$|-,0\rangle \sim -(g/\Delta)|\downarrow,0\rangle + |\uparrow,1\rangle, \quad (7)$$

$$|+,0\rangle \sim |\downarrow,0\rangle + (g/\Delta)|\uparrow,1\rangle. \quad (8)$$

The corresponding decay rates are then simply given by

$$\Gamma_{-,0} \approx (g/\Delta)^2 \gamma + \kappa, \quad (9)$$

$$\Gamma_{+,0} \approx \gamma + (g/\Delta)^2 \kappa. \quad (10)$$

More insight into the dispersive regime is gained by making the unitary transformation

$$U = \exp\left[\frac{g}{\Delta}(a\sigma^+ - a^\dagger\sigma^-)\right] \quad (11)$$

and expanding to second order in g (neglecting damping for the moment) to obtain

$$UHU^\dagger \approx \hbar\left[\omega_r + \frac{g^2}{\Delta}\sigma^z\right]a^\dagger a + \frac{\hbar}{2}\left[\Omega + \frac{g^2}{\Delta}\right]\sigma^z. \quad (12)$$

As is clear from this expression, the atom transition is ac Stark/Lamb shifted by $(g^2/\Delta)(n+1/2)$. Alternatively, one can interpret the ac Stark shift as a dispersive shift of the cavity transition by $\sigma^z g^2/\Delta$. In other words, the atom pulls the cavity frequency by $\pm g^2/\kappa\Delta$.

III. CIRCUIT IMPLEMENTATION OF CAVITY QED

We now consider the proposed realization of cavity QED using the superconducting circuits shown in Fig. 2. A 1D transmission line resonator consisting of a full-wave section of superconducting coplanar waveguide plays the role of the cavity and a superconducting qubit plays the role of the atom. A number of superconducting quantum circuits could function as artificial atom, but for definiteness we focus here on the Cooper-pair box [6,16–18].

A. Cavity: Coplanar stripline resonator

An important advantage of this approach is that the zero-point energy is distributed over a very small effective volume ($\approx 10^{-5}$ cubic wavelengths) for our choice of a quasi-one-dimensional transmission line “cavity.” As shown in Appendix A, this leads to significant rms voltages $V_{\text{rms}}^0 \sim \sqrt{\hbar\omega_r/cL}$ between the center conductor and the adjacent ground plane at the antinodal positions, where L is the resonator length and c is the capacitance per unit length of the transmission line. At a resonant frequency of 10 GHz ($h\nu/k_B \sim 0.5$ K) and for a $10\ \mu\text{m}$ gap between the center conductor and the adjacent ground plane, $V_{\text{rms}} \sim 2\ \mu\text{V}$ corresponding to electric fields $\mathcal{E}_{\text{rms}} \sim 0.2\ \text{V/m}$, some 100 times larger than achieved in the 3D cavity described in Ref. [3]. Thus, this geometry might also be useful for coupling to Rydberg atoms [19].

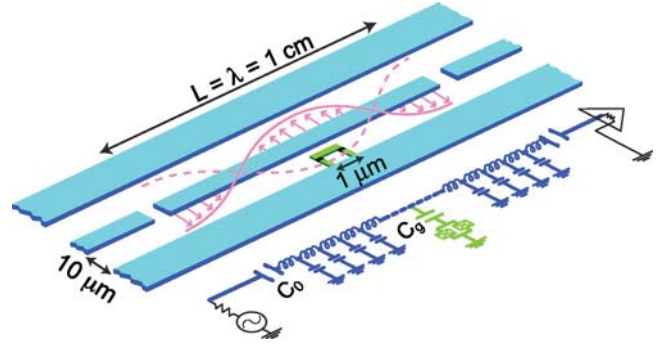


FIG. 2. (Color online). Schematic layout and equivalent lumped circuit representation of proposed implementation of cavity QED using superconducting circuits. The 1D transmission line resonator consists of a full-wave section of superconducting coplanar waveguide, which may be lithographically fabricated using conventional optical lithography. A Cooper-pair box qubit is placed between the superconducting lines and is capacitively coupled to the center trace at a maximum of the voltage standing wave, yielding a strong electric dipole interaction between the qubit and a single photon in the cavity. The box consists of two small ($\sim 100\ \text{nm} \times 100\ \text{nm}$) Josephson junctions, configured in a $\sim 1\ \mu\text{m}$ loop to permit tuning of the effective Josephson energy by an external flux Φ_{ext} . Input and output signals are coupled to the resonator, via the capacitive gaps in the center line, from $50\ \Omega$ transmission lines which allow measurements of the amplitude and phase of the cavity transmission, and the introduction of dc and rf pulses to manipulate the qubit states. Multiple qubits (not shown) can be similarly placed at different antinodes of the standing wave to generate entanglement and two-bit quantum gates across distances of several millimeters.

In addition to the small effective volume and the fact that the on-chip realization of CQED shown in Fig. 2 can be fabricated with existing lithographic techniques, a transmission-line resonator geometry offers other practical advantages over lumped LC circuits or current-biased large Josephson junctions. The qubit can be placed within the cavity formed by the transmission line to strongly suppress the spontaneous emission, in contrast to a lumped LC circuit, where without additional special filtering, radiation and parasitic resonances may be induced in the wiring [20]. Since the resonant frequency of the transmission line is determined primarily by a fixed geometry, its reproducibility and immunity to $1/f$ noise should be superior to Josephson junction plasma oscillators. Finally, transmission-line resonances in coplanar waveguides with $Q \sim 10^6$ have already been demonstrated [21,22], suggesting that the internal losses can be very low. The optimal choice of the resonator Q in this approach is strongly dependent on the intrinsic decay rates of superconducting qubits which, as described below, are presently unknown, but can be determined with the setup proposed here. Here we assume the conservative case of an overcoupled resonator with a $Q \sim 10^4$, which is preferable for the first experiments.

B. Artificial atom: The Cooper-pair box

Our choice of “atom,” the Cooper-pair box [6,16], is a mesoscopic superconducting island. As shown in Fig. 3, the

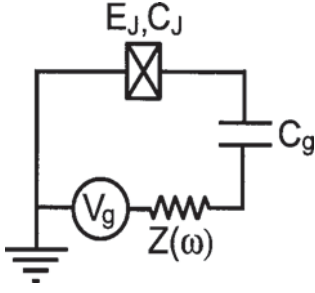


FIG. 3. Circuit diagram of the Cooper-pair box. The gate voltage is connected to the island through an environmental impedance $Z(\omega)$.

island is connected to a large reservoir through a Josephson junction with Josephson energy E_J and capacitance C_J . It is voltage biased from a lead having capacitance C_g to the island. If the superconducting gap is larger than both the charging energy $E_c = e^2/2C_\Sigma$ (where $C_\Sigma = C_J + C_g$ is the total box capacitance) and temperature, the only relevant degree of freedom is the number of Cooper pairs N on the island. In this basis, the Hamiltonian describing the superconducting island takes the form

$$H_Q = 4E_c \sum_N (N - N_g)^2 |N\rangle\langle N| - \frac{E_J}{2} \sum_N (|N+1\rangle\langle N| + \text{H.c.}), \quad (13)$$

where $N_g = C_g V_g / 2e$ is the dimensionless gate charge representing the total polarization charge injected into the island by the voltage source.

In the charge regime $4E_c \gg E_J$ and restricting the gate charge to the range $N_g \in [0, 1]$, only a pair of adjacent charge states on the island are relevant and the Hamiltonian then reduces to a 2×2 matrix

$$H_Q = -\frac{E_{\text{el}}}{2} \bar{\sigma}^z - \frac{E_J}{2} \bar{\sigma}^x, \quad (14)$$

with $E_{\text{el}} = 4E_c(1 - 2N_g)$. The Cooper-pair box can in this case be mapped to a pseudospin-1/2 particle, with effective fields in the x and z directions.

Replacing the Josephson junction by a pair of junctions in parallel, each with energy $E_J/2$, the effective field in the x direction becomes $E_J \cos(\pi \Phi_{\text{ext}} / \Phi_0) / 2$. By threading a flux Φ_{ext} in the loop formed by the pair of junctions and changing the gate voltage V_g , it is possible to control the effective fields acting on the qubit. In the setup of Fig. 2, application of dc gate voltage on the island can be conveniently achieved by applying a bias voltage to the center conductor of the transmission line. The resonator coupling capacitance C_0 , the gate capacitance C_g (the capacitance between the center conductor of the resonator and the island), and the capacitance to ground of the resonator then act as a voltage divider.

C. Combined system: Superconducting cavity QED

For a superconducting island fabricated inside a resonator, in addition to a dc part V_g^{dc} , the gate voltage has a quantum

part v . As shown in Appendix A, if the qubit is placed in the center of the resonator, this latter contribution is given by $v = V_{\text{rms}}^0 (a^\dagger + a)$. Taking into account both V_g^{dc} and v in Eq. (14), we obtain

$$H_Q = -2E_c(1 - 2N_g^{\text{dc}}) \bar{\sigma}^z - \frac{E_J}{2} \bar{\sigma}^x - e \frac{C_g}{C_\Sigma} \sqrt{\frac{\hbar \omega_r}{Lc}} (a^\dagger + a) \times (1 - 2N_g - \bar{\sigma}^z). \quad (15)$$

Working in the eigenbasis $\{|\uparrow\rangle, |\downarrow\rangle\}$ of the first two terms of the above expression [23] and adding the Hamiltonian of the oscillator mode coupled to the qubit, the Hamiltonian of the interacting qubit and resonator system takes the form

$$H = \hbar \omega_r \left(a^\dagger a + \frac{1}{2} \right) + \frac{\hbar \Omega}{2} \sigma^z - e \frac{C_g}{C_\Sigma} \sqrt{\frac{\hbar \omega_r}{Lc}} (a^\dagger + a) \times [1 - 2N_g - \cos(\theta) \sigma^z + \sin(\theta) \sigma^x]. \quad (16)$$

Here, σ^x and σ^z are Pauli matrices in the eigenbasis $\{|\uparrow\rangle, |\downarrow\rangle\}$, $\theta = \arctan[E_J/4E_c(1 - 2N_g^{\text{dc}})]$ is the mixing angle, and the energy splitting of the qubit is $\Omega = \sqrt{E_J^2 + [4E_c(1 - 2N_g^{\text{dc}})]^2} / \hbar$ [23]. Note that contrary to the case of a qubit fabricated outside the cavity where the N_g^2 term in Eq. (13) has no effect, here this term slightly renormalizes the cavity frequency ω_r and displaces the oscillator coordinate. These effects are implicit in Eq. (16).

At the charge degeneracy point (where $N_g^{\text{dc}} = C_g V_g^{\text{dc}} / 2e = 1/2$ and $\theta = \pi/2$), neglecting rapidly oscillating terms and omitting damping for the moment, Eq. (16) reduces to the Jaynes-Cummings Hamiltonian (1) with $\Omega = E_J / \hbar$ and coupling

$$g = \frac{\beta e}{\hbar} \sqrt{\frac{\hbar \omega_r}{cL}}, \quad (17)$$

where $\beta \equiv C_g / C_\Sigma$. The quantum electrical circuit of Fig. 2 is therefore mapped to the problem of a two-level atom inside a cavity. Away from the degeneracy point, this mapping can still be performed, but with a coupling strength reduced by $\sin(\theta)$ and an additional term proportional to $(a^\dagger + a)$.

In this circuit, the ‘‘atom’’ is highly polarizable at the charge degeneracy point, having transition dipole moment $d \equiv \hbar g / \mathcal{E}_{\text{rms}} \sim 2 \times 10^4$ atomic units (ea_0), or more than an order of magnitude larger than even a typical Rydberg atom [15]. An experimentally realistic [18] coupling $\beta \sim 0.1$ leads to a vacuum Rabi rate $g / \pi \sim 100$ MHz, which is three orders of magnitude larger than in corresponding atomic microwave CQED experiments [3] or approximately 1% of the transition frequency. Unlike the usual CQED case, these artificial ‘‘atoms’’ remain at fixed positions indefinitely and so do not suffer from the problem that the coupling g varies with position in the cavity.

A comparison of the experimental parameters for implementations of cavity QED with optical and microwave atomic systems and for the proposed implementation with superconducting circuits is presented in Table I. We assume here a relatively low $Q = 10^4$ and a worst case estimate, con-

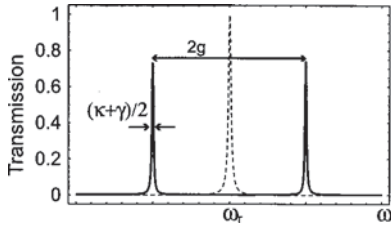


FIG. 4. Expected transmission spectrum of the resonator in the absence (dashed line) and presence (solid line) of a superconducting qubit biased at its degeneracy point. Parameters are those presented in Table I. The splitting exceeds the line width by two orders of magnitude.

sistent with the bound set by previous experiments with superconducting qubits (discussed further below), for the intrinsic qubit lifetime of $1/\gamma \geq 2 \mu\text{s}$.

The standard figures of merit [24] for strong coupling are the critical photon number needed to saturate the atom on resonance, $m_0 = \gamma^2/2g^2 \leq 1 \times 10^{-6}$, and the minimum atom number detectable by measurement of the cavity output, $N_0 = 2\gamma\kappa/g^2 \leq 6 \times 10^{-5}$. These remarkably low values are clearly very favorable and show that superconducting circuits could access the interesting regime of very strong coupling.

IV. ZERO DETUNING

In the case of a low- Q cavity ($g < \kappa$) and zero detuning, the radiative decay rate of the qubit into the transmission line becomes strongly *enhanced* by a factor of Q relative to the rate in the absence of the cavity [15]. This is due to the resonant enhancement of the density of states at the atomic transition frequency. In electrical engineering language, the $\sim 50\Omega$ external transmission-line impedance is transformed on resonance to a high value which is better matched to extract energy from the qubit.

For strong coupling $g > \kappa, \gamma$, the first excited state becomes a doublet with linewidth $(\kappa + \gamma)/2$, as explained in Sec. II. As can be seen from Table I, the coupling in the proposed superconducting implementation is so strong that, even for the low $Q=10^4$ we have assumed, $2g/(\kappa + \gamma) \sim 100$ vacuum Rabi oscillations are possible. Moreover, as shown in Fig. 4, the frequency splitting ($g/\pi \sim 100$ MHz) will be readily resolvable in the transmission spectrum of the resonator. This spectrum, calculated here following Ref. [25], can be observed in the same manner as employed in optical atomic experiments, with a continuous-wave measurement at low drive, and will be of practical use to find the dc gate voltage needed to tune the box into resonance with the cavity.

Of more fundamental importance than this simple avoided level crossing, however, is the fact that the Rabi splitting scales with the square root of the photon number, making the level spacing anharmonic. This should cause a number of novel nonlinear effects [14] to appear in the spectrum at higher drive powers when the average photon number in the cavity is large ($\langle n \rangle > 1$).

A conservative estimate of the noise energy for a 10 GHz cryogenic high-electron-mobility (HEMT) amplifier is $n_{\text{amp}} = k_B T_N / \hbar \omega_r \sim 100$ photons, where T_N is the noise temperature of the amplification circuit. As a result, these spectral features should be readily observable in a measurement time $t_{\text{meas}} = 2n_{\text{amp}} / \langle n \rangle \kappa$ or only $\sim 32 \mu\text{s}$ for $\langle n \rangle \sim 1$.

V. LARGE DETUNING: LIFETIME ENHANCEMENT

For qubits *not* inside a cavity, fluctuation of the gate voltage acting on the qubit is an important source of relaxation and dephasing. As shown in Fig. 3, in practice the qubit's gate is connected to the voltage source through external wiring having, at the typical microwave transition frequency of the qubit, a real impedance of value close to the impedance of free space ($\sim 50 \Omega$). The relaxation rate expected from purely quantum fluctuations across this impedance (spontaneous emission) is [18,23]

$$\frac{1}{T_1} = \frac{E_J^2}{E_J^2 + E_{\text{el}}^2} \left(\frac{e}{\hbar} \right)^2 \beta^2 S_V(+\Omega), \quad (18)$$

where $S_V(+\Omega) = 2\hbar\Omega \text{Re}[Z(\Omega)]$ is the spectral density of voltage fluctuations across the environmental impedance (in the quantum limit). It is difficult in most experiments to precisely determine the real part of the high-frequency environmental impedance presented by the leads connected to the qubit, but reasonable estimates [18] yield values of T_1 in the range of $1 \mu\text{s}$.

For qubits fabricated inside a cavity, the noise across the environmental impedance does not couple directly to the qubit, but only indirectly through the cavity. For the case of strong detuning, coupling of the qubit to the continuum is therefore substantially reduced. One can view the effect of the detuned resonator as filtering out the vacuum noise at the qubit transition frequency or, in electrical engineering terms, as providing an impedance transformation which strongly *reduces* the real part of the environmental impedance seen by the qubit.

Solving for the normal modes of the resonator and transmission lines, including an input impedance R at each end of the resonator, the spectrum of voltage fluctuations as seen by the qubit fabricated in the center of the resonator can be shown to be well approximated by

$$S_V(\Omega) = \frac{2\hbar\omega_r}{Lc} \frac{\kappa/2}{\Delta^2 + (\kappa/2)^2}. \quad (19)$$

Using this transformed spectral density in Eq. (18) and assuming a large detuning between the cavity and qubit, the relaxation rate due to vacuum fluctuations takes a form that reduces to $1/T_1 \equiv \gamma_\kappa = (g/\Delta)^2 \kappa \sim 1/(64 \mu\text{s})$, at the qubit's degeneracy point. This is the result already obtained in Eq. (10) using the dressed-state picture for the coupled atom and cavity, except for the additional factor γ reflecting a loss of energy to modes outside of the cavity. For large detuning, damping due to spontaneous emission can be much less than κ .

One of the important motivations for this CQED experiment is to determine the various contributions to the qubit

decay rate so that we can understand their fundamental physical origins as well as engineer improvements. Besides γ_κ evaluated above, there are two additional contributions to the total damping rate $\gamma = \gamma_\kappa + \gamma_\perp + \gamma_{\text{NR}}$. Here γ_\perp is the decay rate into photon modes other than the cavity mode and γ_{NR} is the rate of other (possibly nonradiative) decays. Optical cavities are relatively open and γ_\perp is significant, but for 1D microwave cavities, γ_\perp is expected to be negligible (despite the very large transition dipole). For Rydberg atoms the two qubit states are both highly excited levels and γ_{NR} represents (radiative) decay out of the two-level subspace. For Cooper-pair boxes, γ_{NR} is completely unknown at the present time, but could have contributions from phonons, two-level systems in insulating [20] barriers and substrates, or thermally excited quasiparticles.

For Cooper box qubits *not* inside a cavity, recent experiments [18] have determined a relaxation time $1/\gamma = T_1 \sim 1.3 \mu\text{s}$ despite the backaction of continuous measurement by a SET electrometer. Vion *et al.* [17] found $T_1 \sim 1.84 \mu\text{s}$ (without measurement backaction) for their charge-phase qubit. Thus, in these experiments, if there are nonradiative decay channels, they are at most comparable to the vacuum radiative decay rate (and may well be much less) estimated using Eq. (18). Experiments with a cavity will present the qubit with a simple and well-controlled electromagnetic environment, in which the radiative lifetime can be enhanced with detuning to $1/\gamma_\kappa > 64 \mu\text{s}$, allowing γ_{NR} to dominate and yielding valuable information about any nonradiative processes.

VI. DISPERSIVE QND READOUT OF QUBITS

In addition to lifetime enhancement, the dispersive regime is advantageous for readout of the qubit. This can be realized by microwave irradiation of the cavity and then probing the transmitted or reflected photons [26].

A. Measurement protocol

A drive of frequency $\omega_{\mu\nu}$ on the resonator can be modeled by [15]

$$H_{\mu\nu}(t) = \hbar \varepsilon(t) (a^\dagger e^{-i\omega_{\mu\nu}t} + a e^{i\omega_{\mu\nu}t}), \quad (20)$$

where $\varepsilon(t)$ is a measure of the drive amplitude. In the dispersive limit, one expects from Fig. 1(c) peaks in the transmission spectrum at $\omega_r - g^2/\Delta$ and $\Omega + 2g^2/\Delta$ if the qubit is initially in its ground state. In a frame rotating at the drive frequency, the matrix elements for these transitions are, respectively,

$$\begin{aligned} \langle \uparrow, 0 | H_{\mu\nu} | \downarrow, n \rangle &\sim \varepsilon, \\ \langle \uparrow, 0 | H_{\mu\nu} | \uparrow, n \rangle &\sim \frac{\varepsilon g}{\Delta}. \end{aligned} \quad (21)$$

In the large detuning case, the peak at $\Omega + 2g^2/\Delta$, corresponding approximately to a qubit flip, is highly suppressed.

The matrix element corresponding to a qubit flip from the excited state is also suppressed and, as shown in Fig. 5,

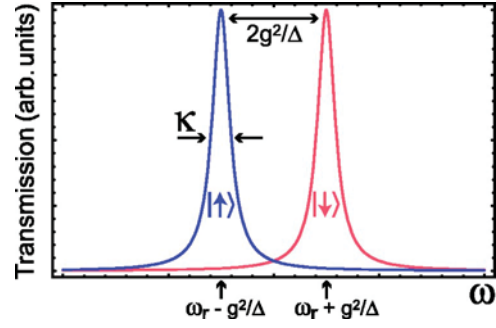


FIG. 5. (Color online) Transmission spectrum of the cavity, which is “pulled” by an amount $\pm g^2/\Delta = \pm 2.5\omega_r \times 10^{-4}$, depending on the state of the qubit (red for the excited state, blue for the ground state). To perform a measurement of the qubit, a pulse of microwave photons, at a probe frequency $\omega_{\mu\nu} = \omega_r$ or $\omega_r \pm g^2/\Delta$, is sent through the cavity. Additional peaks near Ω corresponding to qubit flips are suppressed by g/Δ .

depending on the qubit being in its ground or excited states, the transmission spectrum will present a peak of width κ at $\omega_r - g^2/\Delta$ or $\omega_r + g^2/\Delta$. With the parameters of Table I, this dispersive pull of the cavity frequency is $\pm g^2/\kappa\Delta = \pm 2.5$ linewidths for a 10% detuning. Exact diagonalization (4) shows that the pull is power dependent and decreases in magnitude for cavity photon numbers on the scale $n = n_{\text{crit}} \equiv \Delta^2/4g^2$. In the regime of nonlinear response, single-atom optical bistability [14] can be expected when the drive frequency is off resonance at low power but on resonance at high power [29].

The state-dependent pull of the cavity frequency by the qubit can be used to entangle the state of the qubit with that of the photons transmitted or reflected by the resonator. For $g^2/\kappa\Delta > 1$, as in Fig. 5, the pull is greater than the linewidth, and irradiating the cavity at one of the pulled frequencies $\omega_r \pm g^2/\Delta$, the transmission of the cavity will be close to unity for one state of the qubit and close to zero for the other [30].

Choosing the drive to be instead at the bare cavity frequency ω_r , the state of the qubit is encoded in the phase of the reflected and transmitted microwaves. An initial qubit state $|\chi\rangle = \alpha|\uparrow\rangle + \beta|\downarrow\rangle$ evolves under microwave irradiation into the entangled state $|\psi\rangle = \alpha|\uparrow, \theta\rangle + \beta|\downarrow, -\theta\rangle$, where $\tan \theta = 2g^2/\kappa\Delta$ and $|\pm\theta\rangle$ are (interaction representation) coherent states with the appropriate mean photon number and opposite phases. In the situation where $g^2/\kappa\Delta \ll 1$, this is the most appropriate strategy.

It is interesting to note that such an entangled state can be used to couple qubits in distant resonators and allow quantum communication [31]. Moreover, if an independent measurement of the qubit state can be made, such states can be turned into photon Schrödinger cats [15].

To characterize these two measurement schemes corresponding to two different choices of the drive frequency, we compute the average photon number inside the resonator \bar{n} and the homodyne voltage on the 50Ω impedance at the output of the resonator. Since the power coupled to the outside of the resonator is $P = \langle n \rangle \hbar \omega_r \kappa / 2 = \langle V_{\text{out}} \rangle^2 / R$, the homodyne voltage can be expressed as $\langle V_{\text{out}} \rangle = \sqrt{R \hbar \omega_r \kappa \langle a + a^\dagger \rangle} / 2$ and is proportional to the real part of the field inside the cavity.

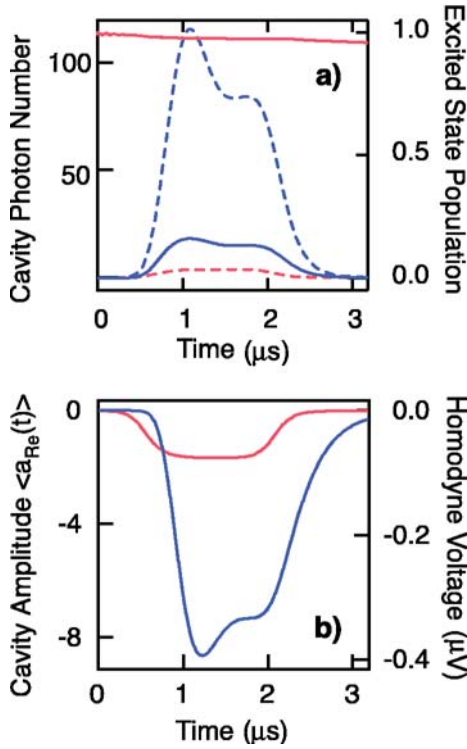


FIG. 6. (Color online) Results of numerical simulations using the quantum-state diffusion method. A microwave pulse of duration $\sim 15/\kappa$ and centered at the pulled frequency $\omega_r + g^2/\Delta$ drives the cavity. (a) The occupation probability of the excited state (right axis, solid lines), for the case in which the qubit is initially in the ground (blue) or excited (red) state and intracavity photon number (left axis, dash lines), are shown as a function of time. Though the qubit states are temporarily coherently mixed during the pulse, the probability of real transitions is seen to be small. Depending on the qubit's state, the pulse is either on or away from the combined cavity-qubit resonance and therefore is mostly transmitted or mostly reflected. (b) The real component of the cavity electric field amplitude (left axis) and the transmitted voltage phasor (right axis) in the output transmission line for the two possible initial qubit states. The parameters used for the simulation are presented in Table I.

In the absence of dissipation, the time dependence of the field inside the cavity can be obtained in the Heisenberg picture from Eqs. (12) and (20). This leads to a closed set of differential equations for a , σ^z , and $a\sigma^z$ which is easily solved. In the presence of dissipation, however [i.e., performing the transformation (11) on H_κ and H_γ , and adding the resulting terms to Eqs. (12) and (20)], the set is no longer closed and we resort to numerical stochastic wave function calculations [32]. See Appendix B for a brief presentation of this numerical method.

Figures 6 and 7 show the numerical results for the two choices of drive frequency and using the parameters of Table I. For these calculations, a pulse of duration $\sim 15/\kappa$ with a hyperbolic tangent rise and fall is used to excite the cavity. Figure 6 corresponds to a drive at the pulled frequency $\omega_r + g^2/\Delta$. In Fig. 6(a) the probability P_1 to find the qubit in its excited state (right axis) is plotted as a function of time for the qubit initially in the ground (blue) or excited state (red). The dashed lines represent the corresponding number of pho-

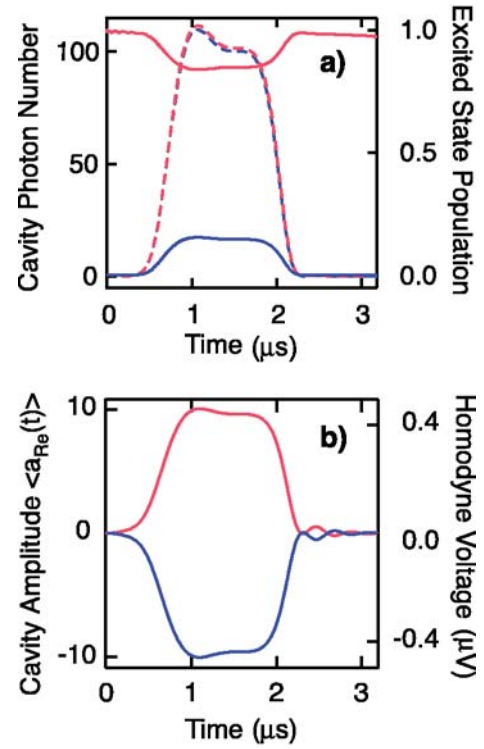


FIG. 7. (Color online) Same as Fig. 6 for the drive at the bare cavity frequency ω_r . Depending on the qubit's state, the pulse is either above or below the combined cavity-qubit resonance and so is partly transmitted and reflected but with a large relative phase shift that can be detected with homodyne detection. In (b), the opposing phase shifts cause a change in sign of the output, which can be measured with high signal to noise to realize a single-shot, QND measurement of the qubit.

tons in the cavity (left axis). Figure 6(b) shows, in a frame rotating at the drive frequency, the real part of the cavity electric field amplitude (left axis) and transmitted voltage phase (right axis) in the output transmission line, again for the two possible initial qubit states. These quantities are shown in Fig. 7 for a drive at the bare frequency ω_r .

As expected, for the first choice of drive frequency, the information about the state of the qubit is mostly stored in the number of transmitted photons. When the drive is at the bare frequency, however, there is very little information in the photon number, with most of the information being stored in the phase of the transmitted and reflected signal. This phase shift can be measured using standard heterodyne techniques. As also discussed in Appendix C, both approaches can serve as a high-efficiency quantum nondemolition dispersive readout of the state of the qubit.

B. Measurement time and backaction

As seen from Eq. (12), the backaction of the dispersive CQED measurement is due to quantum fluctuations of the number of photons n within the cavity. These fluctuations cause variations in the ac Stark shift $(g^2/\Delta)n\sigma^z$, which in turn dephase the qubit. It is useful to compute the corresponding dephasing rate and compare it with the measure-

ment rate—i.e., the rate at which information about the state of the qubit can be acquired.

To determine the dephasing rate, we assume that the cavity is driven at the bare cavity resonance frequency and that the pull of the resonance is small compared to the linewidth κ . The relative phase accumulated between the ground and excited states of the qubit is

$$\varphi(t) = 2 \frac{g^2}{\Delta} \int_0^t dt' n(t'), \quad (22)$$

which yields a mean phase advance $\langle \varphi \rangle = 2\theta_0 N$ with $\theta_0 = 2g^2/\kappa\Delta$ and $N = \kappa\bar{n}t/2$ the total number of transmitted photons [14]. For weak coupling, the dephasing time will greatly exceed $1/\kappa$ and, in the long-time limit, the noise in φ induced by the ac Stark shift will be Gaussian. Dephasing can then be evaluated by computing the long-time decay of the correlator

$$\begin{aligned} \langle \sigma^+(t) \sigma^-(0) \rangle &= \left\langle \exp \left(i \int_0^t dt' \varphi(t') \right) \right\rangle \\ &\simeq \exp \left[-\frac{1}{2} \left(2 \frac{g^2}{\Delta} \right)^2 \int_0^t \int_0^t dt_1 dt_2 \langle n(t_1) n(t_2) \rangle \right]. \end{aligned} \quad (23)$$

To evaluate this correlator in the presence of a continuous-wave (cw) drive on the cavity, we first perform a canonical transformation on the cavity operators $a^{(\dagger)}$ by writing them in terms of a classical $\alpha^{(*)}$ and a quantum part $d^{(\dagger)}$:

$$a(t) = \alpha(t) + d(t). \quad (24)$$

Under this transformation, the coherent state obeying $a|\alpha\rangle = \alpha|\alpha\rangle$ is simply the vacuum for the operator d . It is then easy to verify that

$$\langle [n(t) - \bar{n}][n(0) - \bar{n}] \rangle = \alpha^2 \langle d(t) d^\dagger(0) \rangle = \bar{n} e^{-\kappa|t|/2}. \quad (25)$$

It is interesting to note that the factor of $1/2$ in the exponent is due to the presence of the coherent drive. If the resonator is not driven, the photon number correlator rather decays at a rate κ . Using this result in Eq. (23) yields the dephasing rate

$$\Gamma_\varphi = 4\theta_0^2 \frac{\kappa}{2} \bar{n}. \quad (26)$$

Since the rate of transmission on resonance is $\kappa\bar{n}/2$, this means that the dephasing per transmitted photon is $4\theta_0^2$.

To compare this result to the measurement time T_{meas} , we imagine a homodyne measurement to determine the transmitted phase. Standard analysis of such an interferometric setup [14] shows that the minimum phase change which can be resolved using N photons is $\delta\theta = 1/\sqrt{N}$. Hence the measurement time to resolve the phase change $\delta\theta = 2\theta_0$ is

$$T_m = \frac{1}{2\kappa\bar{n}\theta_0^2}, \quad (27)$$

which yields

$$T_m \Gamma_\varphi = 1. \quad (28)$$

This exceeds the quantum limit [33] $T_m \Gamma_\varphi = 1/2$ by a factor of 2. Equivalently, in the language of Ref. [34] (which uses a definition of the measurement time twice as large as that above) the efficiency ratio is $\chi \equiv 1/(T_m \Gamma_\varphi) = 0.5$.

The failure to reach the quantum limit can be traced [35] to the fact that the coupling of the photons to the qubit is not adiabatic. A small fraction $R \approx \theta_0^2$ of the photons incident on the resonator are reflected rather than transmitted. Because the phase shift of the reflected wave [14] differs by π between the two states of the qubit, it turns out that, despite its weak intensity, the reflected wave contains precisely the same amount of information about the state of the qubit as the transmitted wave which is more intense but has a smaller phase shift. In the language of Ref. [34], this “wasted” information accounts for the excess dephasing relative to the measurement rate. By measuring also the phase shift of the reflected photons, it could be possible to reach the quantum limit.

Another form of possible backaction is mixing transitions between the two qubit states induced by the microwaves. First, as seen from Fig. 6(a) and 7(a), increasing the average number of photons in the cavity induces mixing. This is simply caused by dressing of the qubit by the cavity photons. Using the dressed states (2) and (3), the level of this coherent mixing can be estimated as

$$P_{\uparrow,\downarrow} = \frac{1}{2} \langle \pm, n | \pm \sigma^z | \pm, n \rangle \quad (29)$$

$$= \frac{1}{2} \left(1 \pm \frac{\Delta}{\sqrt{4g^2(n+1) + \Delta^2}} \right). \quad (30)$$

Exciting the cavity to $n = n_{\text{crit}}$ yields $P_{\downarrow} \sim 0.85$. As is clear from the numerical results, this process is completely reversible and does not lead to errors in the readout.

The drive can also lead to real transitions between the qubit states. However, since the coupling is so strong, large detuning $\Delta = 0.1 \omega_r$ can be chosen, making the mixing rate limited not by the frequency spread of the drive pulse, but rather by the width of the qubit excited state itself. The rate of driving the qubit from ground to excited state when n photons are in the cavity is $R \approx n(g/\Delta)^2 \gamma$. If the measurement pulse excites the cavity to $n = n_{\text{crit}}$, we see that the excitation rate is still only $1/4$ of the relaxation rate. As a result, the main limitation on the fidelity of this QND readout is the decay of the excited state of the qubit during the course of the readout. This occurs (for small γ) with probability $P_{\text{relax}} \sim \gamma t_{\text{meas}} \sim 15\gamma/\kappa \sim 3.75\%$ and leads to a small error $P_{\text{err}} \sim 5\gamma/\kappa \sim 1.5\%$ in the measurement, where we have taken $\gamma = \gamma_\kappa$. As confirmed by the numerical calculations of Fig. 6 and 7, this dispersive measurement is therefore highly nondemolition.

C. Signal to noise

For homodyne detection in the case where the cavity pull $g^2/\Delta\kappa$ is larger than 1, the signal-to-noise ratio (SNR) is given by the ratio of the number of photons, $n_{\text{sig}} = n\kappa\Delta t/2$,

TABLE II. Figures of merit for readout and multiqubit entanglement of superconducting qubits using dispersive (off-resonant) coupling to a 1D transmission-line resonator. The same parameters as Table I and a detuning of the Cooper-pair box from the resonator of 10% ($\Delta=0.1\omega_r$) are assumed. Quantities involving the qubit decay γ are computed both for the theoretical lower bound $\gamma=\gamma_\kappa$ for spontaneous emission via the cavity and (in parentheses) for the current experimental upper bound $1/\gamma\geq 2\ \mu\text{s}$. Though the signal to noise of the readout is very high in either case, the estimate of the readout error rate is dominated by the probability of qubit relaxation during the measurement, which has a duration of a few cavity lifetimes $[\sim(1-10)\kappa^{-1}]$. If the qubit nonradiative decay is low, both high-efficiency readout and more than 10^3 two-bit operations could be attained.

Parameter	Symbol	1D circuit
Dimensionless cavity pull	$g^2/\kappa\Delta$	2.5
Cavity-enhanced lifetime	$\gamma_\kappa^{-1}=(\Delta/g)^2\kappa^{-1}$	64 μs
Readout SNR	$\text{SNR} = (n_{\text{crit}}/n_{\text{amp}})\kappa/2\gamma$	200 (6)
Readout error	$P_{\text{err}}\sim 5\times\gamma/\kappa$	1.5% (14%)
One-bit operation time	$T_\pi > 1/\Delta$	>0.16 ns
Entanglement time	$t_{\sqrt{\text{ISWAP}}} = \pi\Delta/4g^2$	$\sim 0.05\ \mu\text{s}$
Two-bit operations	$N_{\text{op}} = 1/[\gamma t_{\sqrt{\text{ISWAP}}}]$	>1200(40)

accumulated over an integration period Δt , divided by the detector noise $n_{\text{amp}}=k_B T_N/\hbar\omega_r$. Assuming the integration time to be limited by the qubit's decay time $1/\gamma$ and exciting the cavity to a maximal amplitude $n_{\text{crit}}=100\sim n_{\text{amp}}$, we obtain $\text{SNR} = (n_{\text{crit}}/n_{\text{amp}})(\kappa/2\gamma)$. If the qubit lifetime is longer than a few cavity decay times ($1/\kappa=160$ ns), this SNR can be very large. In the most optimistic situation where $\gamma=\gamma_\kappa$, the signal-to-noise ratio is $\text{SNR}=200$.

When taking into account the fact that the qubit has a finite probability to decay during the measurement, a better strategy than integrating the signal for a long time is to take advantage of the large SNR to measure quickly. Simulations have shown that in the situation where $\gamma=\gamma_\kappa$, the optimum integration time is roughly 15 cavity lifetimes. This is the pulse length used for the stochastic numerical simulations shown above. The readout fidelity, including the effects of this stochastic decay, and related figures of merit of the single-shot high efficiency QND readout are summarized in Table II.

This scheme has other interesting features that are worth mentioning here. First, since nearly all the energy used in this dispersive measurement scheme is dissipated in the remote terminations of the input and output transmission lines, it has the practical advantage of avoiding quasiparticle generation in the qubit.

Another key feature of the cavity QED readout is that it lends itself naturally to operation of the box at the charge degeneracy point ($N_g=1/2$), where it has been shown that T_2 can be enormously enhanced [17] because the energy splitting has an extremum with respect to gate voltage and isolation of the qubit from $1/f$ dephasing is optimal. The derivative of the energy splitting with respect to gate voltage is the charge difference in the two qubit states. At the degeneracy point this derivative vanishes and the environment cannot

distinguish the two states and thus cannot dephase the qubit. This also implies that a charge measurement cannot be used to determine the state of the system [4,5]. While the first derivative of the energy splitting with respect to gate voltage vanishes at the degeneracy point, the second derivative, corresponding to the difference in charge *polarizability* of the two quantum states, is *maximal*. One can think of the qubit as a nonlinear quantum system having a state-dependent capacitance (or in general, an admittance) which changes sign between the ground and excited states [36]. It is this change in polarizability which is measured in the dispersive QND measurement.

In contrast, standard charge measurement schemes [37,18] require moving away from the optimal point. Simmonds *et al.* [20] have recently raised the possibility that there are numerous parasitic environmental resonances which can relax the qubit when its frequency Ω is changed during the course of moving the operating point. The dispersive CQED measurement is therefore highly advantageous since it operates best at the charge degeneracy point. In general, such a measurement of an ac property of the qubit is strongly desirable in the usual case where dephasing is dominated by low-frequency ($1/f$) noise. Notice also that the proposed quantum nondemolition measurement would be the inverse of the atomic microwave CQED measurement in which the state of the photon field is inferred nondestructively from the phase shift in the state of atoms sent through the cavity [3].

VII. COHERENT CONTROL

While microwave irradiation of the cavity at its resonance frequency constitutes a measurement, irradiation close to the qubit's frequency can be used to coherently control the state of the qubit. In the former case, the phase shift of the transmitted wave is strongly dependent on the state of the qubit and hence the photons become entangled with the qubit, as shown in Fig. 8. In the latter case, however, driving is *not* a measurement because, for large detuning, the photons are largely reflected with a phase shift which is independent of the state of the qubit. There is therefore little entanglement between the field and qubit in this situation and the rotation fidelity is high.

To model the effect of the drive on the qubit, we add the microwave drive of Eq. (20) to the Jaynes-Cummings Hamiltonian (1) and apply the transformation (11) (again neglecting damping) to obtain the effective one-qubit Hamiltonian

$$H_{1q} = \frac{\hbar}{2} \left[\Omega + 2 \frac{g^2}{\Delta} \left(a^\dagger a + \frac{1}{2} \right) - \omega_{\mu w} \right] \sigma^z + \hbar \frac{g\varepsilon(t)}{\Delta} \sigma^x + \hbar(\omega_r - \omega_{\mu w}) a^\dagger a + \hbar\varepsilon(t)(a^\dagger + a) \quad (31)$$

in a frame rotating at the drive frequency $\omega_{\mu w}$. Choosing $\omega_{\mu w} = \Omega + (2n+1)g^2/\Delta$, H_{1q} generates rotations of the qubit about the x axis with Rabi frequency $g\varepsilon/\Delta$. Different drive frequencies can be chosen to realize rotations around arbitrary axes in the x - z plane. In particular, choosing $\omega_{\mu w} = \Omega + (2n+1)g^2/\Delta - 2g\varepsilon/\Delta$ and $t = \pi\Delta/2\sqrt{2}g\varepsilon$ generates the Hadamard transformation H . Since $H\sigma^x H = \sigma^z$, these two choices

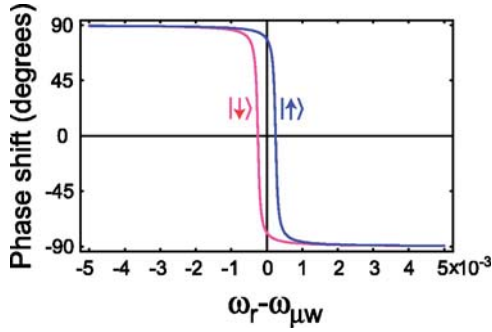


FIG. 8. (Color online) Phase shift of the cavity field for the two states of the qubit as a function of detuning between the driving and resonator frequencies. Obtained from the steady-state solution of the equation of motion for $a(t)$ while only taking into account damping on the cavity and using the parameters of Table I. Readout of the qubit is realized at, or close to, zero detuning between the drive and resonator frequencies where the dependence of the phase shift on the qubit state is largest. Coherent manipulations of the qubit are realized close to the qubit frequency which is 10% detuned from the cavity (not shown on this scale). At such large detunings, there is little dependence of the phase shift on the qubit's state.

of frequency are sufficient to realize any one-qubit logical operation.

Assuming that we can take full advantage of lifetime enhancement inside the cavity (i.e., that $\gamma = \gamma_c$), the number of π rotations about the x axis which can be carried out is $N_\pi = 2\varepsilon\Delta / \pi g \kappa \sim 10^5 \varepsilon$ for the experimental parameters assumed in Table I. For large ε , the choice of drive frequency must take into account the power dependence of the cavity frequency pulling.

Numerical simulation shown in Fig. 9 confirms this simple picture and that single-bit rotations can be performed with very high fidelity. It is interesting to note that since detuning between the resonator and the drive is large, the cavity is only virtually populated, with an average photon

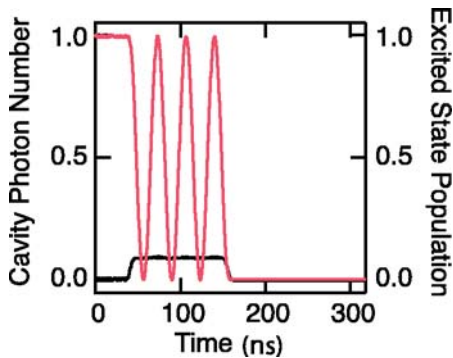


FIG. 9. (Color online) Numerical stochastic wave function simulation showing coherent control of a qubit by microwave irradiation of the cavity at the ac Stark- and Lamb-shifted qubit frequency. The qubit (red line) is first left to evolve freely for about 40 ns. The drive is turned on for $t = 7\pi\Delta / 2g\varepsilon \sim 115$ ns, corresponding to 7π pulses, and then turned off. Since the drive is tuned far away from the cavity, the cavity photon number (black line) is small even for the moderately large drive amplitude $\varepsilon = 0.03 \omega_r$ used here.

number $\bar{n} \approx \varepsilon^2 / \Delta^2 \sim 0.1$. Virtual population and depopulation of the cavity can be realized much faster than the cavity lifetime $1/\kappa$ and, as a result, the qubit feels the effect of the drive rapidly after the drive has been turned on. The limit on the speed of turn on and off of the drive is set by the detuning Δ . If the drive is turned on faster than $1/\Delta$, the frequency spread of the drive is such that part of the drive's photons will pick up phase information (see Fig. 8) and dephase the qubit. As a result, for large detuning, this approach leads to a fast and accurate way to coherently control the state of the qubit.

To model the effect of the drive on the resonator an alternative model is to use the cavity-modified Maxwell-Bloch equations [25]. As expected, numerical integration of the Maxwell-Bloch equations reproduce very well the stochastic numerical results when the drive is at the qubit's frequency but do *not* reproduce these numerical results when the drive is close to the bare resonator frequency (Figs. 6 and 7)—i.e., when entanglement between the qubit and photons cannot be neglected.

VIII. RESONATOR AS QUANTUM BUS: ENTANGLEMENT OF MULTIPLE QUBITS

The transmission-line resonator has the advantage that it should be possible to place multiple qubits along its length (~ 1 cm) and entangle them together, which is an essential requirement for quantum computation. For the case of two qubits, they can be placed closer to the ends of the resonator but still well isolated from the environment and can be separately dc biased by capacitive coupling to the left and right center conductors of the transmission line. Additional qubits would have to have separate gate bias lines installed.

For the pair of qubits labeled i and j , both coupled with strength g to the cavity and detuned from the resonator but in resonance with each other, the transformation (11) yields the effective two-qubit Hamiltonian [3,38,39]

$$H_{2q} \approx \hbar \left[\omega_r + \frac{g^2}{\Delta} (\sigma_i^z + \sigma_j^z) \right] a^\dagger a + \frac{1}{2} \hbar \left[\Omega + \frac{g^2}{\Delta} \right] (\sigma_i^z + \sigma_j^z) + \hbar \frac{g^2}{\Delta} (\sigma_i^+ \sigma_j^- + \sigma_i^- \sigma_j^+). \quad (32)$$

In addition to ac Stark and Lamb shifts, the last term couples the qubits through virtual excitations of the resonator.

In a frame rotating at the qubit's frequency Ω , H_{2q} generates the evolution

$$U_{2q}(t) = \exp \left[-i \frac{g^2}{\Delta} t \left(a^\dagger a + \frac{1}{2} \right) (\sigma_i^z + \sigma_j^z) \right] \times \begin{pmatrix} 1 & & & \\ & \cos \frac{g^2}{\Delta} t & i \sin \frac{g^2}{\Delta} t & \\ & i \sin \frac{g^2}{\Delta} t & \cos \frac{g^2}{\Delta} t & \\ & & & 1 \end{pmatrix} \otimes \mathbb{1}_r, \quad (33)$$

where $\mathbb{1}_r$ is the identity operator in resonator space. Up to

phase factors, this corresponds at $t = \pi\Delta/4g^2 \sim 50$ ns to a $\sqrt{i\text{SWAP}}$ logical operation. Up to one-qubit gates, this operation is equivalent to the controlled-NOT gate. Together with one-qubit gates, the interaction H_{2q} is therefore sufficient for universal quantum computation [40]. Assuming again that we can take full advantage of the lifetime enhancement inside the cavity, the number of $\sqrt{i\text{SWAP}}$ operations which can be carried out is $N_{2q} = 4\Delta/\pi\kappa \sim 1200$ for the parameters assumed above. This can be further improved if the qubit's nonradiative decay is sufficiently small and higher Q cavities are employed.

When the qubits are detuned from each other, the off-diagonal coupling provided by H_{2q} is only weakly effective and the coupling is for all practical purposes turned off. Two-qubit logical gates in this setup can therefore be controlled by individually tuning the qubits. Moreover, single-qubit and two-qubit logical operations on different qubits and pairs of qubits can both be realized simultaneously, a requirement to reach presently known thresholds for fault-tolerant quantum computation [41].

It is interesting to point out that the dispersive QND readout presented in Sec. VI may be able to determine the state of multiple qubits in a single shot without the need for additional signal ports. For example, for the case of two qubits with different detunings, the cavity pull will take four different values $\pm g_1^2/\Delta_1 \pm g_2^2/\Delta_2$, allowing single-shot readout of the coupled system. This can in principle be extended to N qubits provided that the range of individual cavity pulls can be made large enough to distinguish all the combinations. Alternatively, one could read them out in small groups at the expense of having to electrically vary the detuning of each group to bring them into strong coupling with the resonator.

IX. ENCODED UNIVERSALITY AND DECOHERENCE-FREE SUBSPACE

Universal quantum computation can also be realized in this architecture under the encoding $\mathcal{L} = \{|\uparrow\downarrow\rangle, |\downarrow\uparrow\rangle\}$ by controlling only the qubit's detuning and, therefore, by turning on and off the interaction term in H_{2q} [42].

An alternative encoded two-qubit logical operation to the one suggested in Ref. [42] can be realized here by tuning the four qubits forming the pair of encoded qubits in resonance for a time $t = \pi\Delta/3g^2$. The resulting effective evolution operator can be written as $\hat{U}_{2q} = \exp[-i(\pi\Delta/3g^2)\hat{\sigma}_{x1}\hat{\sigma}_{x2}]$, where $\hat{\sigma}_{xi}$ is a Pauli operator acting on the i th encoded qubit. Together with encoded one-qubit operations, \hat{U}_{2q} is sufficient for universal quantum computation using the encoding \mathcal{L} .

We point out that the subspace \mathcal{L} is a decoherence-free subspace with respect to global dephasing [43] and use of this encoding will provide some protection against noise. The application of \hat{U}_{2q} on the encoded subspace \mathcal{L} , however, causes temporary leakage out of this protected subspace. This is also the case with the approach of Ref. [42]. In the present situation, however, since the Hamiltonian generating \hat{U}_{2q} commutes with the generator of global dephasing, this temporary excursion out of the protected subspace does not induce noise on the encoded qubit.

X. SUMMARY AND CONCLUSIONS

In summary, we propose that the combination of one-dimensional superconducting transmission-line resonators, which confine their zero-point energy to extremely small volumes, and superconducting charge qubits, which are electrically controllable qubits with large electric dipole moments, constitutes an interesting system to access the strong-coupling regime of cavity quantum electrodynamics. This combined system is an advantageous architecture for the coherent control, entanglement, and readout of quantum bits for quantum computation and communication. Among the practical benefits of this approach are the ability to suppress radiative decay of the qubit while still allowing one-bit operations, a simple and minimally disruptive method for readout of single and multiple qubits, and the ability to generate tunable two-qubit entanglement over centimeter-scale distances. We also note that in the structures described here, the emission or absorption of a single photon by the qubit is tagged by a sudden large change in the resonator transmission properties [29], making them potentially useful as single-photon sources and detectors.

ACKNOWLEDGEMENTS

We are grateful to David DeMille, Michel Devoret, Clifford Cheung, and Florian Marquardt for useful conversations. We also thank André-Marie Tremblay and the Canadian Foundation for Innovation for access to computing facilities. This work was supported in part by the National Security Agency (NSA) and Advanced Research and Development Activity (ARDA) under Army Research Office (ARO) Contract No. DAAD19-02-1-0045, NSF DMR-0196503, NSF DMR-0342157, the NSF ITR program under Grant No. DMR-0325580, the David and Lucile Packard Foundation, the W.M. Keck Foundation, and NSERC.

APPENDIX A: QUANTIZATION OF THE 1D TRANSMISSION-LINE RESONATOR

A transmission line of length L , whose cross-section dimension is much less than the wavelength of the transmitted signal, can be approximated by a 1D model. For relatively low frequencies it is well described by an infinite series of inductors with each node capacitively connected to ground, as shown in Fig. 2. Denoting the inductance per unit length l and the capacitance per unit length c , the Lagrangian of the circuit is

$$\mathcal{L} = \int_{-L/2}^{L/2} dx \left(\frac{l}{2} j^2 - \frac{1}{2c} q^2 \right), \quad (\text{A1})$$

where $j(x, t)$ and $q(x, t)$ are the local current and charge density, respectively. We have ignored for the moment the two semi-infinite transmission lines capacitively coupled to the resonator. Defining the variable $\theta(x, t)$,

$$\theta(x, t) \equiv \int_{-L/2}^x dx' q(x', t), \quad (\text{A2})$$

the Lagrangian can be rewritten as

$$L = \int_{-L/2}^{L/2} dx \left(\frac{l}{2} \dot{\theta}^2 - \frac{1}{2c} (\nabla \theta)^2 \right). \quad (\text{A3})$$

The corresponding Euler-Lagrange equation is a wave equation with the speed $v = \sqrt{l/c}$. Using the boundary conditions due to charge neutrality,

$$\theta(-L/2, t) = \theta(L/2, t) = 0, \quad (\text{A4})$$

we obtain

$$\begin{aligned} \theta(x, t) = & \sqrt{\frac{2}{L}} \sum_{k_o=1}^{k_o, \text{cutoff}} \phi_{k_o}(t) \cos \frac{k_o \pi x}{L} \\ & + \sqrt{\frac{2}{L}} \sum_{k_e=2}^{k_e, \text{cutoff}} \phi_{k_e}(t) \sin \frac{k_e \pi x}{L}, \end{aligned} \quad (\text{A5})$$

for odd and even modes, respectively. For finite length L , the transmission line acts as a resonator with resonant frequencies $\omega_k = k\pi v/L$. The cutoff is determined by the fact that the resonator is not strictly one dimensional.

Using the normal-mode expansion (A5) in (A3), one obtains, after spatial integration, the Lagrangian in the form of a set of harmonic oscillators:

$$\mathcal{L} = \sum_k \frac{l}{2} \dot{\phi}_k^2 - \frac{1}{2c} \left(\frac{k\pi}{L} \right)^2 \phi_k^2. \quad (\text{A6})$$

Promoting the variable ϕ_k and its canonically conjugated momentum $\pi_k = l\dot{\phi}_k$ to conjugate operators and introducing the boson creation and annihilation operators a_k^\dagger and a_k satisfying $[a_k, a_{k'}^\dagger] = \delta_{kk'}$, we obtain the usual relations diagonalizing the Hamiltonian obtained from the Lagrangian (A6):

$$\hat{\phi}_k(t) = \sqrt{\frac{\hbar \omega_k c}{2}} \frac{L}{k\pi} [a_k(t) + a_k^\dagger(t)], \quad (\text{A7})$$

$$\hat{\pi}_k(t) = -i \sqrt{\frac{\hbar \omega_k l}{2}} [a_k(t) - a_k^\dagger(t)]. \quad (\text{A8})$$

From these relations, the voltage on the resonator can be expressed as

$$\begin{aligned} V(x, t) = & \frac{1}{c} \frac{\partial \theta(x, t)}{\partial x} \\ = & - \sum_{k_o=1}^{\infty} \sqrt{\frac{\hbar \omega_{k_o}}{Lc}} \sin \left(\frac{k_o \pi x}{L} \right) [a_{k_o}(t) + a_{k_o}^\dagger(t)] \\ & + \sum_{k_e=1}^{\infty} \sqrt{\frac{\hbar \omega_{k_e}}{Lc}} \cos \left(\frac{k_e \pi x}{L} \right) [a_{k_e}(t) + a_{k_e}^\dagger(t)]. \end{aligned} \quad (\text{A9})$$

In the presence of the two semi-infinite transmission lines coupled to the resonator, the Lagrangian (A3) and the boundary conditions (A4) are modified to take into account the voltage drop on the coupling capacitors C_0 . Assuming no spatial extent for the capacitors C_0 , the problem is still solvable analytically. Due to this coupling, the wave function can

now extend outside of the central segment which causes a slight redshift, of order C_0/Lc , of the cavity resonant frequency.

As shown in Fig. 2, we assume the qubit to be fabricated at the center of the resonator. As a result, at low temperatures, the qubit is coupled to the mode $k=2$ of the resonator, which as an antinode of the voltage in its center. The rms voltage between the center conductor and the ground plane is then $V_{\text{rms}}^0 = \sqrt{\hbar \omega_r / cL}$ with $\omega_r = \omega_2$ and the voltage felt by the qubit is $V(0, t) = V_{\text{rms}}^0 [a_2(t) + a_2^\dagger(t)]$. In the main body of this paper, we work only with this second harmonic and drop the mode index on the resonator operators.

APPENDIX B: TREATMENT OF DISSIPATION

The evolution of the total density matrix, including the qubit, cavity mode, and baths, is described by the von Neuman equation

$$\dot{\rho}_{\text{tot}} = -\frac{i}{\hbar} [H_{\text{sys}} + H_\kappa + H_\gamma, \rho_{\text{tot}}], \quad (\text{B1})$$

where H_{sys} stands for the first three terms of Eq. (1) plus the drive Hamiltonian of Eq. (20). An explicit expression for H_κ can be found in Ref. [14]. When the coupling between the system (qubit plus cavity mode) and the baths is weak, the reduced density operator for the system can be shown to obey the master equation [14]

$$\dot{\rho} = -\frac{i}{\hbar} [H_{\text{sys}}, \rho] - \frac{1}{2} \sum_{m=\{\kappa, \gamma\}} (L_m^\dagger L_m \rho + \rho L_m^\dagger L_m - 2L_m \rho L_m^\dagger) \quad (\text{B2})$$

in the Markov approximation. Here, L_m are Lindblad operators describing the effect of the baths on the system and can be expressed as $L_\kappa = \sqrt{\kappa} a$ and $L_\gamma = \sqrt{\gamma} \sigma^-$. The effect of finite temperature and pure dephasing, for example, can also be taken into account easily by introducing additional Lindblad operators.

The master equation is solved numerically by truncating the cavity Hilbert space to N photons. This leads to $(2N)^2$ coupled differential equations which, for large N , can be difficult to solve in practice. An alternative approach is to write an equivalent stochastic differential equation for the wave function [32,44]. There exist different such ‘‘unravelings’’ of the master equation and here we use the quantum state diffusion equation [32,44]

$$\begin{aligned} |d\psi\rangle = & -\frac{i}{\hbar} H_{\text{sys}} |\psi\rangle dt + \sum_m (L_m - \langle L_m \rangle_\psi) |\psi\rangle d\xi_m \\ & - \frac{1}{2} \sum_m (L_m^\dagger L_m + \langle L_m^\dagger \rangle_\psi \langle L_m \rangle_\psi - 2\langle L_m^\dagger \rangle_\psi \langle L_m \rangle_\psi) |\psi\rangle dt. \end{aligned} \quad (\text{B3})$$

The $d\xi_m$ are complex independent Wiener processes satisfying for their ensemble averages

$$\overline{d\xi_m} = \overline{d\xi_m d\xi_n} = 0, \quad (\text{B4})$$

$$\overline{d\xi_m^* d\xi_n} = \delta_{mn} dt. \quad (\text{B5})$$

An advantage of this approach is that now only $2N$ coupled differential equations have to be solved. A drawback is that the results must be averaged over many realizations of the noise to obtain accurate results. Still, this leads to much less important memory usage and to speedup in the numerical calculations [32,45].

APPENDIX C: QUANTUM NONDEMOLITION MEASUREMENTS

Readout of a qubit can lead to both mixing and dephasing [23,33]. While dephasing is unavoidable, mixing of the measured observable can be eliminated in a QND measurement by choosing the qubit-measurement apparatus interaction such that the measured observable is a constant of motion. In that situation, the measurement-induced mixing is rather introduced in the operator conjugate to the operator being measured.

In the situation of interest in this paper, the operator being probed is σ^z and, from Eq. (12), the qubit-measurement apparatus interaction Hamiltonian is given for large detuning by $H_{\text{int}} = (g^2/\Delta)\sigma^z a^\dagger a$, such that $[\sigma^z, H_{\text{int}}] = 0$. For σ^z to be a constant of motion also requires that it commute with the qubit Hamiltonian. This condition is also satisfied in Eq. (12).

That the measured observable is a constant of motion implies that repeated observations will yield the same result. This allows for the measurement result to reach arbitrary large accuracy by accumulating signal. In practice, however, there are always environmental dissipation mechanisms acting on the qubit independently of the readout. Even in a QND situation, these will lead to a finite mixing rate $1/T_1$ of the qubit in the course of the measurement. Hence, high fidelity can only be achieved by a strong measurement completed in a time $T_m \ll T_1$. This simple point is not as widely appreciated as it should be.

-
- [1] H. Mabuchi and A. Doherty, *Science* **298**, 1372 (2002).
 [2] C. J. Hood, T. W. Lynn, A. C. Doherty, A. S. Parkins, and H. J. Kimble, *Science* **287**, 1447 (2000).
 [3] J. Raimond, M. Brune, and S. Haroche, *Rev. Mod. Phys.* **73**, 565 (2001).
 [4] A. Armour, M. Blencowe, and K. C. Schwab, *Phys. Rev. Lett.* **88**, 148301 (2002).
 [5] E. K. Irish and K. Schwab, *Phys. Rev. B* **68**, 155311 (2003).
 [6] Y. Makhlin, G. Schön, and A. Shnirman, *Rev. Mod. Phys.* **73**, 357 (2001).
 [7] O. Buisson and F. Hekking, in *Macroscopic Quantum Coherence and Quantum Computing*, edited by D. V. Averin, B. Ruggiero, and P. Silvestrini (Kluwer, New York, 2001).
 [8] F. Marquardt and C. Bruder, *Phys. Rev. B* **63**, 054514 (2001).
 [9] F. Plastina and G. Falci, *Phys. Rev. B* **67**, 224514 (2003).
 [10] A. Blais, A. Maassen van den Brink, and A. Zagoskin, *Phys. Rev. Lett.* **90**, 127901 (2003).
 [11] W. Al-Saidi and D. Stroud, *Phys. Rev. B* **65**, 014512 (2001).
 [12] C.-P. Yang, S.-I. Chu, and S. Han, *Phys. Rev. A* **67**, 042311 (2003).
 [13] J. Q. You and F. Nori, *Phys. Rev. B* **68**, 064509 (2003).
 [14] D. Walls and G. Milburn, *Quantum Optics* (Springer-Verlag, Berlin, 1994).
 [15] S. Haroche, in *Fundamental Systems in Quantum Optics*, edited by J. Dalibard, J. Raimond, and J. Zinn-Justin (Elsevier, New York, 1992), p. 767.
 [16] V. Bouchiat, D. Vion, P. Joyez, D. Esteve, and M. Devoret, *Phys. Scr.* **T76**, 165 (1998).
 [17] D. Vion, A. Aassime, A. Cottet, P. Joyez, H. Pothier, C. Urbina, D. Esteve, and M. Devoret, *Science* **296**, 886 (2002).
 [18] K. Lehnert, K. Bladth, L. Spietz, D. Gunnarsson, D. Schuster, P. Delsing, and R. Schoelkopf, *Phys. Rev. Lett.* **90**, 027002 (2003).
 [19] A. S. Sørensen, C. H. van der Wal, L. Childress, and M. D. Lukin, *Phys. Rev. Lett.* **92**, 063601 (2004).
 [20] R. W. Simmonds, K. M. Lang, D. A. Hite, D. P. Pappas, and J. Martinis (unpublished).
 [21] P. K. Day, H. G. LeDuc, B. A. Mazin, A. Vayonakis, and J. Zmuidzinas, *Nature (London)* **425**, 817 (2003).
 [22] A. Wallraff and R. Schoelkopf (unpublished).
 [23] R. Schoelkopf, A. Clerk, S. Girvin, K. Lehnert, and M. Devoret, *Quantum Noise in Mesoscopic Physics* (Kluwer Academic, Dordrecht, 2003), Chap. 9, pp. 175–203.
 [24] H. Kimble, *Cavity Quantum Electrodynamics* (Academic Press, San Diego, 1994).
 [25] C. Wang and R. Vyas, *Phys. Rev. A* **55**, 823 (1997).
 [26] A lumped LC circuit was used in Refs. [27,28] to probe flux qubits in a different way.
 [27] E. Il'ichev, N. Oukhanski, A. Izmalkov, T. Wagner, M. Grajcar, H.-G. Meyer, A. Y. Smirnov, A. Maassen van den Brink, M. Amin, and A. Zagoskin, *Phys. Rev. Lett.* **91**, 097906 (2003).
 [28] A. Izmalkov, M. Grajcar, E. Il'ichev, T. Wagner, H.-G. Meyer, A. Smirnov, M. Amin, A. Maassen van den Brink, and A. Zagoskin, eprint cond-mat/0312332.
 [29] S. Girvin, A. Blais, and R. Huang (unpublished).
 [30] We note that for the case of $Q=10^6$, the cavity pull is a remarkable ± 250 linewidths, but depending on the nonradiative decay rate of the qubit, this may be in the regime $\kappa < \gamma$, making the state measurement too slow.
 [31] S. van Enk, J. Cirac, and P. Zoller, *Science* **279**, 2059 (1998).
 [32] R. Schack and T. A. Brun, *Comput. Phys. Commun.* **102**, 210 (1997).
 [33] M. Devoret and R. Schoelkopf, *Nature (London)* **406**, 1039 (2000).
 [34] A. Clerk, S. Girvin, and A. Stone, *Phys. Rev. B* **67**, 165324 (2003).
 [35] F. Marquardt (unpublished).
 [36] D. Averin and C. Bruder, *Phys. Rev. Lett.* **91**, 057003 (2003).
 [37] Y. Nakamura, Y. Pashkin, and J. Tsai, *Nature (London)* **398**, 786 (1999).
 [38] A. Sørensen and K. Mølmer, *Phys. Rev. Lett.* **82**, 1971 (1999).

- [39] S.-B. Zheng and G.-C. Guo, *Phys. Rev. Lett.* **85**, 2392 (2000).
- [40] A. Barenco, C. Bennett, R. Cleve, D. DiVincenzo, N. Margolus, S. P. T. Sleator, J. Smolin, and H. Weinfurter, *Phys. Rev. A* **52**, 3457 (1995).
- [41] D. Aharonov and M. Ben-Or, in *Proceedings of the 37th Annual Symposium on Foundations of Computer Science* (IEEE Computer Society Press, Los Alamitos, CA, 1996), p. 46.
- [42] D. Lidar and L.-A. Wu, *Phys. Rev. Lett.* **88**, 017905 (2002).
- [43] J. Kempe, D. Bacon, D. Lidar, and K. B. Whaley, *Phys. Rev. A* **63**, 042307 (2001).
- [44] C. Gardiner and P. Zoller, *Quantum Noise* (Springer-Verlag, Berlin, 2000).
- [45] K. Molmer, Y. Castin, and J. Dalibard, *J. Opt. Soc. Am. B* **10**, 524 (1993).